

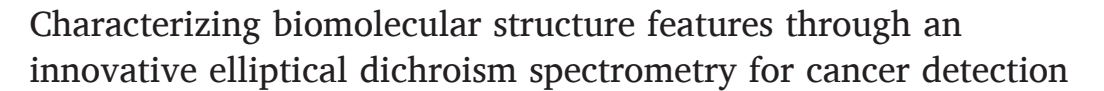
Contents lists available at ScienceDirect

Heliyon

journal homepage: www.cell.com/heliyon



Research article





- ^a Biomedical Engineering Program, North Dakota State University, 1401 Centennial Blvd, Engineering Administration, Room 203, Fargo, ND, 58102, United States
- ^b Materials and Nanotechnology, North Dakota State University, Fargo, ND 58108, United States
- ^c Department of Aerospace Engineering, Iowa State University, Ames, IA, 50011, United States
- d Department of Electrical and Computer Engineering, North Dakota State University, 1411 Centennial Blvd., 101S Fargo, ND, 58102, United States
- e Department of Electrical & Computer Engineering, University of Denver, 2155 E. Wesley Ave., Denver, CO, 80210, United States
- f Knoebel Institute for Healthy Aging, University of Denver, United States

ARTICLE INFO

Keywords: Elliptical dichroism Spectrometer Stereochemical analysis Tumor differentiation Autocorrelation function Density-functional theory Molecular dynamics simulation

ABSTRACT

This research introduces a novel method for evaluating the structural features of biomolecules, utilizing our innovative Elliptical Dichroism (ED) spectrometer specifically designed for stereochemical analysis. By integrating ED spectrometry with autocorrelation (AC) analysis, we investigate the conformational characteristics of biological molecules such as amino acids, proteins, and extracellular vesicles (EVs) induced by elliptically polarized UV absorption. Our streamlined approach offers a cost-effective and portable solution with minimal sample consumption and supports multiple working modes to efficiently characterize biomolecular structures. The insight from this new approach demonstrates potential applications in using biomolecular characterization for cancer detection.

1. Introduction

Understanding the structure and function of biological molecules, such as amino acids, proteins, and EVs, is essential in studying biological processes [1,2]. The conformational alterations of these molecules impact their behavior, playing a significant role in both healthy and pathological conditions. Precisely assessing these conformational changes is crucial for the progress of biophysics and medicine [3,4]. Prominent methods such as X-ray crystallography, nuclear magnetic resonance (NMR) spectroscopy, cryo-electron microscopy (Cryo-EM), hydrogen-deuterium exchange mass spectrometry (HDX-MS), Fourier-transform infrared spectroscopy (FTIR), fluorescence spectroscopy, and circular dichroism (CD) spectroscopy have been applied in unraveling the structural characteristics of biomolecules. Each technique offers unique advantages, ranging from the high-resolution atomic-level structural analysis provided by X-ray crystallography to probe protein dynamics in solution through NMR spectroscopy [5,6]. Cryo-EM allows for the

https://doi.org/10.1016/j.heliyon.2024.e38399

^{*} Corresponding author. Knoebel Institute for Healthy Aging, Department of Electrical & Computer Engineering, University of Denver, 2155 E. Wesley Ave., Denver, CO, 80210, United States.

E-mail address: dali.sun@du.edu (D. Sun).

¹ These authors contributed equally.

visualization of flexible and dynamic biomolecules at near-atomic resolution, while HDX-MS identifies regions experiencing conformational changes [7,8]. FTIR provides insights into secondary structure elements, fluorescence spectroscopy enables sensitive detection of structural changes, and CD spectroscopy is valuable for assessing protein folding and secondary structure [9–11]. Despite their merits, these techniques have limitations such as lengthy sample pre-processing, complicated data analysis, and high-cost instrumentation. Therefore, it is essential to develop simpler and more efficient techniques to bridge the existing gaps in evaluating biomolecular structures.

In our previous study, we created an elliptical dichroism (ED) spectrometer that uses the absorption of left- and right-circularly polarized light, providing a simplified method to study the structural characteristics of biomolecules [12]. In this previous study we have validated the ED spectrometer's use for secondary structural analysis. Based off its closely related homologue, the CD spectrometer, this ED spectrometer combined a linear polarizer and a rotating waveplate to construct elliptically and circularly polarized light. Ideally, when utilizing a rotating quarter waveplate (rotating angle θ), the elliptically polarized light should follow a repeating pattern associated with angle θ . Using elliptically polarized light provides more comprehensive data and reduces ambiguities compared to conventional linearly polarized light, enhancing the observation of molecular dynamics and interactions. Accordingly, the analyte's absorbance should display radial symmetry from θ 0 to θ 180. However, we observed absorbance asymmetry in certain samples (Figs. S1, S2, and S3). Since the rotator is motorized, a large angle enables longer light exposure. This led us to hypothesize if the asymmetry observed is due to inherent characteristics of the biomolecules or prolonged UV light exposure. Since biomolecules with varying structural features respond differently to UV exposure, we may utilize the asymmetrical outlook of ED spectrometry as a method for structural characterization. To investigate this possibility, we tested various biomolecules and biological samples with the ED spectrometer, aiming to investigate the correlation between the observed asymmetry and the stereochemical features present in these samples.

In this study, we employed integrated two-dimensional Autocorrelation (AC) in the ED spectrometry readouts as an innovative approach to detect and quantify asymmetry in absorption peaks. AC, in the context of our research, refers to a signal processing technique, analyzes absorption peak symmetry by comparing characteristics within the first 0°-180° of the circular spectra to those in the subsequent 180°. High AC values, indicating symmetrical absorption profiles, suggest the absence of structural changes induced by UV-polarized light. Conversely, low AC values denote asymmetry, signaling potential structural alterations in the biomolecules. This innovative application of AC in ED spectrometry provides insights into biomolecular structural transformations under UV exposure. To validate the efficacy of AC for structural characterization, we conducted absorption measurements, quantum mechanical simulations, and molecular dynamics simulations (mean square displacement, MSD) on various biomolecules. These comprehensive investigations established a significant correlation between the stereochemical characteristics of biomolecules and their AC readouts, underscoring the potential of AC-enhanced ED spectrometry in advanced biomolecular research. By extension, we also evaluated the potential application of ED stereochemical analysis in cancer diagnosis. Our study demonstrates the ED spectrometer's potential as an accessible alternative for evaluating the structural features of biomolecules, offering benefits such as low sample consumption, user-friendly operation, and multiple working modes. Moreover, we explored using AC from the ED spectrometer to characterize biological samples. By measuring medium, cell lysates, and EVs, we observed significant differences in AC readouts between non-malignant and malignant samples, suggesting its potential application in cancer detection. This method allows collective attributes, rather than single markers, to report disease states, such as an increased beta-sheet presence in tumorous cells and EVs [13-15]. Our new AC approach with the ED spectrometer extends its capabilities for stereochemical analysis, establishing it as an innovative and versatile tool for structure characterization. Notably, our technique's application to cancer detection showcases its ability to identify structural changes in disease-related biomolecules, potentially serving as a reliable method for noninvasive disease detection and enhancing patient prognosis. However, while highlighting the potential of integrating AC analysis with the ED spectrometer for biomolecular research and cancer detection, represents an initial step. It establishes a foundation for future work focused on optimizing this method for clinical diagnostic applications. Our aim is to further develop and refine the ED spectrometer, enhancing its utility as a vital tool in clinical diagnostics.

2. Experimental section

2.1. Experimental setup

The absorption-based ED instrument setup involves an intricate light path and optics assembly (detail in the previous paper [12]). Starting with a deuterium lamp (Hamamatsu) as the light source, the light was controlled using a lever-actuated iris (Thorlabs) before being collimated by a UV-fused silica collimator lens (Thorlabs). The collimated light undergoes linear polarization using a Glan-Taylor prism polarizer (Edmund Optics), and the polarization state is adjusted by a quarter waveplate (Karl Lambrecht Corporation), which connects to a compact electrical motorized rotator. The light is ultimately detected by a GaP switchable gain amplified detector (Thorlabs), with all these components mounted on an $8" \times 10"$ aluminum breadboard (Thorlabs). The assembly also features a 3D-printed sample holder for a quartz cuvette (Hellma) which ensures liquid sample is held perpendicular to the light path. With the use of a UV deuterium lamp, the entire peptide bond absorption range is covered since the lamp encompasses a range between 185 and 400 nm. The system is housed within a pneumatically sealed aluminum cage connected to a vacuum system for effective heat dissipation and ozone ventilation. Control and data acquisition is managed via a laptop, which connects to the waveplate motor via USB and the light detector through a digital oscilloscope (TBS1000C, Tektronix). The oscilloscope functions as an analog-to-digital converter, facilitating data acquisition. Custom software drives the motor and collects light-intensity data simultaneously, with each measurement taken five times for each rotation angle of the waveplate to enhance accuracy. Furthermore, elliptical light symmetricity

validated by simulation and stability testing was employed in our previous research [12] showing stable readout over multiple days. Employing AC analysis with this setup effectively demonstrates its capability to discern pronounced changes in the second half of the absorption peaks. To illustrate this, a line is drawn from 0° to 180° of the peaks, as shown in the AC analysis in Fig. 1. This line serves as an illustrative guide in the AC analysis, providing a quantitative basis for the comparative assessment of the absorption peak's segments. The changes observed, presumably resulting from prolonged exposure to UV-polarized light, indicate alterations in the molecular structure of the analyte. Consequently, our devised AC method emerges as a potent tool for detecting and quantifying biomolecular structural transformations.

2.2. ED measurement

Amino acid and protein samples were prepared in phosphate-buffered saline (PBS, pH 7.0) at 1 mg/mL and 0.5 mg/mL concentrations, respectively. 200 μ L of the solution was loaded into the sample cuvette covered with a lid for the measurements. The system was turned on 30 min prior to each measurement for stable readout. Before measuring samples, the solvent solution was measured five times and averaged as the blank, which corrected the impact from all optical components (e.g., quartz cuvette) or from any inherent mechanical movement in the light path. Each sample was measured five times as well. The absorbance was normalized to the blank using $A(\theta) = log\left(\frac{I_{blank}(\theta)}{I_{sample}(\theta)}\right)$. In the Angle sweep (AS) mode, the baseline was corrected by a simple straight line linear subtraction connecting the starting and ending points. In the ED mode, ED value was calculated as $ED = A_l - A_r$, where A_l and A_r are absorbance at left and right elliptical polarization ($\theta = 45^{\circ}$ and 135°), respectively. Left and right elliptical polarized light difference achieves one value which is coined as ED value. Data analysis and graphing were performed using Origin Pro 2022. Measurements of amino acids, proteins, and biological samples in AS mode are summarized in Figs. S1, S2, and S3 respectively.

2.3. UV spectrophotometer measurements

The UV Absorption (Ab) measurement was recorded using a SpectraMax Plus 384 (Molecular Devices, LLC, USA) with a cylindrical cuvette of 0.1 cm thickness. Amino acid and protein samples were prepared in PBS (pH 7.0), at 1 mg/mL and 0.5 mg/mL

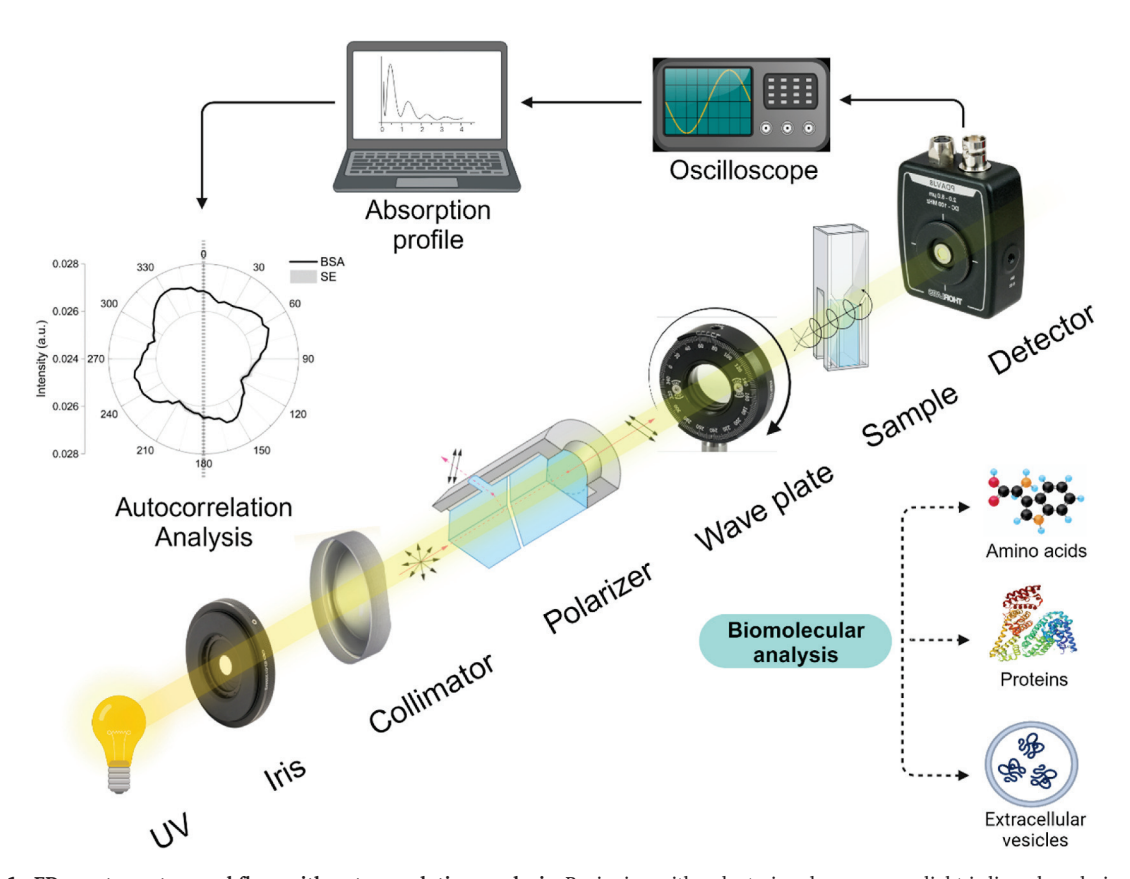


Figure 1. ED spectrometry workflow with autocorrelation analysis. Beginning with a deuterium lamp source, light is linearly polarized, then transformed into elliptically polarized light via a rotating waveplate. The light interacts with the biomolecular sample before reaching the detector, providing the absorption profile. Autocorrelation analysis of this profile enables the structural characterization of biomolecules, including amino acids, proteins, and extracellular vesicles.

concentrations, respectively. The samples were quantified by measuring absorption at 280 nm measured with a Nanodrop ND-1000 spectrophotometer (Thermo Fisher Scientific Inc., USA). 300 μ L of the solution was loaded into the sample cuvette with a lid to measure Ab scan at 200–400 nm wavelength region. Three scans were averaged for each Ab spectrum. Data were analyzed and processed using Origin Pro 2022. Ab measurements of the amino acids and proteins are summarized in Fig. S4 and Fig. S5, respectively.

2.4. Electronic circular dichroism (ECD) spectra simulation

All density functional theory (DFT) calculations were performed by the Gaussian09 program package at 298 K. Initially, molecular structures of amino acids were optimized to their ground state using Becke's three-parameter hybrid B3LYP exchange-correlation functional and double-zeta polarized 6-31G(d) basis set, which provides accurate description of valence electrons, their polarization effects and good balance between accuracy and computational efficiency [16,17,18]. Using the optimized geometries and at the same theory level, the Time-Dependent Density Functional Theory (TD-DFT) was employed to calculate excitation energy (eV), excitation wavelength (nm), and rotatory strength R in the dipole velocity (R_{vel}) and dipole length (R_{len}) components [19]. Next, the ECD spectra, $\Delta \in (L \text{ mol}^{-1} \text{ cm}^{-1})$, were defined as the difference between the left and right molar absorptivity of circularly polarized light and calculated using the following Gaussian function [20]

$$\Delta \in (E) = \frac{1}{2.297 \times 10^{-39}} \ \frac{1}{\sqrt{2\pi\sigma}} \ \sum_{j}^{A} \Delta E_{j} R_{j} e^{[-(E - \Delta E_{j}/2\sigma)]^{2}}$$

where σ (eV) represents half of the bandwidth at 1/e height. E_j (eV) and R_j (10⁻⁴⁰ cgs) represent the excitation energies and rotatory strengths for transition j, respectively. In this study, $\sigma = 0.33$ eV and R_{vel} were used. Simulated ECD spectra of amino acids are shown in Fig. S6.

2.5. Mean square displacement (MSD) simulation

All the atomistic molecular dynamics (AA-MD) simulations of amino acids and proteins are conducted using the GROMACS software package using CHARMM36 force field [21]. Initial structures of amino acids, bovine serum albumin (BSA, 6RJV), avidin (7P4Z), chymotrypsin (4H4F), and xylanase (1K45) were protonated and solved using TIP4P model (https://www.rcsb.org/). The simulation box was set with a minimum distance of 1.2 nm between the protein and the box edges, and periodic boundary conditions were applied in all three dimensions. Following the building of initial configuration, all systems went through an energy minimization step using steepest descent algorithm to eliminate conformational overlap, followed by 100 ps MD simulation with NPT ensemble [22]. The NPT ensemble allows the study of pressure effects on biological system by enabling volume fluctuations, making simulations directly comparable to experimental results and crucial for understanding structural changes in proteins. The temperatures of amino acids and proteins are maintained constant at 310 K by Berendsen thermostat. Position restraints were applied on heavy protein atoms during equilibration to equilibrate solvent, and unrestrained production simulations were run for 100 ns with a 2 fs time step, saving trajectories every 10 ps for further analysis. To quantify the stability of structures $< r^2(t) >$ a property indicative of fast dynamics is measured. In our simulation, we compute MSD using the following equation:

$$< r^{2}(t) > = \langle |r_{i}(t) - r_{i}(0)|^{2} \rangle$$

where $|r_j|(t)$ is the position of j th particles at time t and ζ ... \rangle represents the ensemble average all the particles. The optimized structures are summarized in Fig. S7. MSD curves of amino acids and proteins as a function of time lag τ (10ps) are shown in Fig. S8 and Fig. S9, respectively.

2.6. Cell lines and cell culture

The human pancreatic cancer cell lines MIA PaCa-2 and HPNE were obtained from the American Type Culture Collection (Manassas, Virginia). MIA PaCa-2 cells were cultured in DMEM High Glucose medium (Hyclone, GE Healthcare Life Sciences), and HPNE cells were cultured in DMEM High Glucose (Hyclone, GE Healthcare Life Sciences) with 0.1 ng/mL epidermal growth factor (EGF, Novus Biologicals, USA). All cultures except the non-starvation conditions were supplemented with 10 % fetal bovine serum (FBS; Life technology, Thermo Scientific Inc.), penicillin (1 U), and streptomycin (1 μ g/mL). All cells were maintained in a humidified incubator with 5 % CO₂ at 37 °C. All cell lines were cultured in triplicate under the same conditions and then harvested to collect independent EV samples. Cell lysates were collected when reached confluence using 100 μ L CellyticTM M cell lysis reagent (Sigma-Aldrich) in the culture dish for 30 min. The total protein content in each sample was quantified by a Nanodrop 1000 spectrometer.

2.7. EV isolation from culture media

Cells were grown in culture media with serum until 10^7 cells were obtained, washed three times with PBS, (pH 7.0) and then cultured for 48 h in serum-free media. For non-starvation conditions, the cells were cultured in a medium with 10 % EV-depleted FBS (Thermo Scientific, US). Culture supernatants were then filtered by a 0.2 μ m filter and centrifuged at 10,000 g for 30 min to remove cell debris. The supernatant was carefully centrifuged at 200,000 g for 70 min. The resulting EV precipitates were collected, dissolved in

 $100 \mu L$ PBS (pH 7.0), and stored at 4 °C. TEM (JEOL JEM-2100) and a tunable resistive pulse sensing instrument (qNano system; IZON Science Ltd, Christchurch, New Zealand) were used to validate EV samples.

2.8. Statistics

Comparisons between the two groups were performed using unpaired two-tailed Mann–Whitney U test for non-normally distributed unpaired samples and paired two-tailed Mann–Whitney U test for paired samples. For normally distributed parameters, a two-tailed student's t-test was employed. Correlation analyses between two sets of data were carried out using Pearson correlation analysis and Spearman's rank-order correlation. Pearson's correlation was used to assess the strength and direction of the linear relationship and results were visualized through a 95 % confidence ellipse. Spearman's correlation coefficient, a non-parametric measure, was used for variables that did not assume a linear relationship and/or did not follow a normal distribution. Pearson and Spearman correlation coefficients and the correlation analyses were performed using Origin Pro 2022 software. Data are presented as either representative examples or as means \pm SEM of 4+ experiments. p-values were obtained using both unpaired two-tailed student's t-test and Mann-Whitney U test. Furthermore, statistical analysis of cell derived samples used non-parametric statistical methods based on five biological repeats of cell sample, ensuring true reflection of differences between subjects. Statistical significance was denoted as follows: *p < 0.05, **p < 0.01, ***p < 0.001, and ****p < 0.0001.

3. Results

3.1. Structural characterization of small biomolecules: amino acids

Amino acids are essential to proper functioning and have even been shown to have treatment efficacy against some types of cancer [23], thus their structure is an important feature to analyze. Amino acids are chiral molecules with molecular asymmetry that is not superimposable on their mirror image [24]. Optical rotation is a renowned method to measure chirality [25]. Our previous study demonstrated the reliability of ED spectrometry in measuring the chirality of amino acids based on differential absorption of left- and right-elliptically polarized light [12]. In this study, we employed our ED spectrometer, operating in AS mode to evaluate the absorbance of soluble L-form amino acids over elliptically polarized light and investigate the link between the structure and the readout from the ED spectrometer (Fig. S1). By integrating a linear polarizer and a rotating waveplate, the ED spectrometer generates elliptically polarized light. In theory, when employing a rotating quarter waveplate (at an angle θ), the elliptically polarized light should exhibit a repeating pattern corresponding to θ . Consequently, the analyte's absorbance should demonstrate symmetricity. Nevertheless, we noticed absorbance asymmetry in different amino acids. The motorized rotator allows for larger angles, extending light

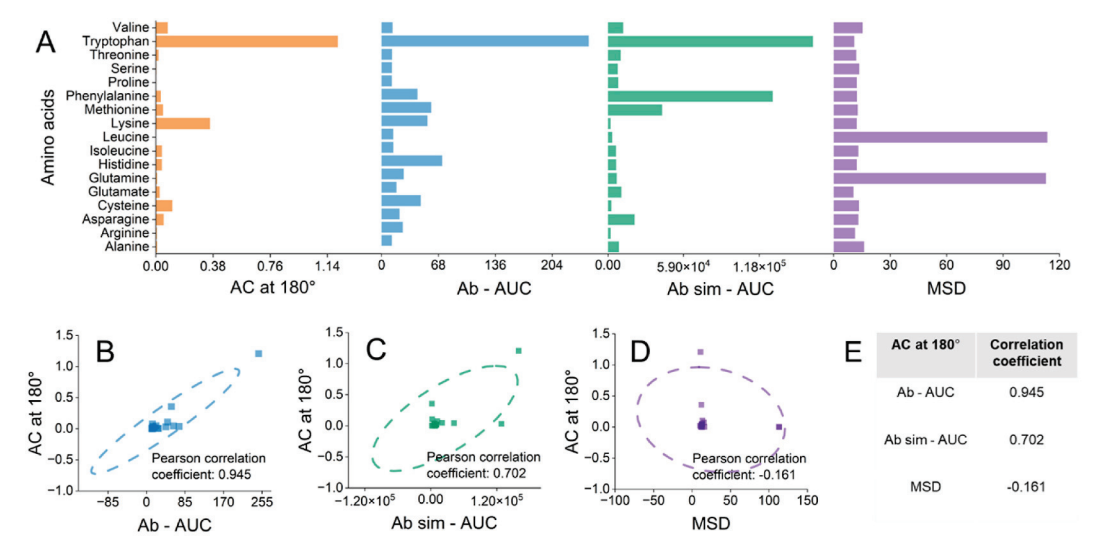


Figure 2. Structural characterization of small biomolecules: amino acids. Analysis of amino acids' structural properties. (A) Autocorrelation at 180° (AC at 180°) indicating structural changes in amino acids, absorption-area under the curve (Ab-AUC) for experimental absorption validation, absorption simulation-area under the curve (Ab sim-AUC) for simulated absorption comparison and, mean square displacement (MSD) at 10ps highlighting vibrational motion and stability dynamics. (B) Pearson's correlation coefficient of 0.945 between AC at 180° and Ab-AUC within a 95% confidence ellipse, showing a strong positive correlation and emphasizing the relationship between structural changes and experimental absorption. (C) Pearson's correlation coefficient of 0.702 between AC at 180° and Ab sim-AUC, linking structural changes with simulated absorption, suggesting AC an indicator of structural variations (0.9 vs 0.7). (D) Pearson's correlation coefficient of -0.161 between AC at 180° and MSD, indicating minimal impact of detected changes on amino acids' vibrational motion and stability. (E) Summarizes correlation coefficients, demonstrating the interplay between structural changes, absorption, and molecular dynamics. The ED spectra for AC were averaged from five repeated measurements. Error bars represent mean \pm s.e.m; n = 4.

exposure periods. Given that biomolecules with diverse structural features respond differently to UV exposure, we proposed using the asymmetry outlook of ED spectrometer readout as a method for structural characterization. To achieve this goal, we utilized autocorrelation at 180° (AC at 180°), a quantitative tool for measuring asymmetry in absorption characteristics over elliptically polarized light (ED). We aimed to investigate the relationship between these samples' observed asymmetry and stereochemical features.

Our methodology relied on the AC at 180° of the ED readout as an indicator for the anticipated symmetric absorbance patterns, supported by the principles of quarter-wave plate functionality. We utilized AC at 180° to discern and quantify the degree of asymmetry and potential structural modifications within the amino acid samples, as shown in Fig. 2A and S10. To validate whether the asymmetric indicator AC can represent structure variation, we utilized a UV spectrophotometer [26] to quantify the UV absorption area under the curve (Ab-AUC) within 200–400 nm (Fig. S4). UV light exposure results in energy absorption by amino acids, leading to electronic transitions and bond rotation. This rotation changes the molecular structure, often favoring a lower-energy state to maintain the conformation of biomolecules [27], which can be used as a structural characterization method.

As shown in Fig. 2A, tryptophan indicated the highest AC at 180° and Ab-AUC values, attributable to its indole ring side chain's conjugated π system, promoting absorption [28]. Nevertheless, its energy dissipated through non-radiative pathways [29] with its rigid side chain resisting conformational changes. Conversely, proline and leucine exhibited lower AC at 180° and Ab-AUC values. Proline's unique pyrrolidine ring structure restricts spatial flexibility during energy absorption, potentially altering its structure [30]. Leucine, lacking a conjugated system and having a flexible side chain [31] absorbs UV light less efficiently, however, UV exposure can lead to structural changes. Lysine and cysteine, like tryptophan, showed high AC at 180° and Ab-AUC values due to their polar charged group influencing absorption through the local field effect [32]. Nonetheless, UV exposure does not induce significant structural changes due to the dissipation of absorbed energy [32,33]. Our investigation showed a strong Pearson's correlation coefficient of 0.945 between AC at 180° from the ED spectrometer and Ab-AUC from the UV spectrophotometer (Fig. 2B and E). The high correlation of Samall biomolecules in the absorbance of polarized light.

To gain a deeper understanding of amino acid structural transformations, we employed quantum mechanical simulation (Ab sim) to model absorption behavior [34] integral to electronic circular dichroism (ECD) spectra, denoted as Ab sim-area under the curve (Ab sim-AUC), as shown in Fig. 2. Ab sim-AUC is sensitive to the structure of biomolecules, providing a detailed view of the spatial arrangement of the amino acids (Fig. S6). We correlated the Ab sim-AUC spectra with AC at 180° results to provide evidence to support using AC to characterize structural variations. Similar to the absorption measurement, tryptophan displayed the highest simulated absorption, attributed to its indole side chain, despite minor structural variation. The conjugated double bonds in the side chain enable substantial electronic delocalization, resulting in a high Ab sim-AUC value. Moreover, tryptophan's high AC at 180° value suggests minimal perturbation within the delocalized π-electron system. Contrarily, lysine's terminal amine group with hydrogen bonds maintains dipole movement [35] and limits structural changes resulting in high AC at 180° value. However, the lack of an extended conjugated system curtails its Ab sim-AUC value. Methionine, marked by its unique thioether side chain, displays substantial absorption, evidenced by its high Ab sim-AUC value. Despite significant structural alterations, reflected in its low AC at 180° value, minor structural shifts driven by the sulfur atom can modify molecular orientation, influencing light absorption and enhancing absorption potential [36]. Phenylalanine, characterized by a flexible aromatic side chain and a conjugated π system, demonstrates a low AC at 180°, signifying substantial structural alterations. This side chain enables electronic delocalization, resulting in a high Ab sim-AUC value. The carbon-carbon bond linking the phenyl ring to the backbone permits significant molecular rotation, enhancing structural changes [37]. Our study reveals a Pearson's correlation of 0.702 between AC at 180° and Ab sim-AUC in amino acids as shown in Fig. 2C and E, linking structural changes to absorption. This observation also raised the potential of using AC to characterize the theoretical structure. Since the AC is more correlated to actual absorption measurement (0.9 vs. 0.7), it is more suitable to indicate true

Mean Square Displacement (MSD) serves as a critical metric for quantifying the vibrational motion of amino acid molecules [38]. In our analysis, we initially measured the displacement of molecules within the system over a short time period of 10 ps (t = 10 ps). This specific time frame is chosen to capture the initial ballistic region of the MSD curve, where the motion is predominantly influenced by the initial conditions and marks the onset of molecular diffusion within the system. Recognizing the importance of broader temporal analysis, our study extends beyond this initial phase to include integration times that span from the nanosecond regime up to microseconds. This comprehensive approach allows us to observe the transition of amino acids from the ballistic to the diffusive region, providing a more complete understanding of their stability. When evaluating the MSD values among the tested amino acids, we observe a diverse range of vibrational motion, correspondings to varying structural stability at 10 ps (Fig. S8). Tryptophan, characterized by a low MSD value, suggests limited vibrational motion due to its rigid indole side chain [39]. This constraint implies minimal structural perturbation, reinforcing its inherent structure. Leucine, with a notably high MSD value, exhibits extensive vibrational motion, likely due to the flexibility of its aliphatic side chain. This flexibility permits substantial molecular movements, potentially causing structural alterations [40]. Elevated MSD values imply significant molecular displacement within an amino acid at 10 ps, often indicating reduced structural stability due to increased dynamic behavior [41]. Interestingly, our analysis reveals a weak correlation coefficient of -0.161 between the AC at 180° of the ED spectra and the amino acid's MSD, as shown in Fig. 2D and E. This negative correlation implies an inverse relationship - increased AC at 180° values, indicating minimal structural changes, correspond to decreased MSD values, and vice versa. The weak correlation strength suggests that changes detected by ED spectrometry do not significantly impact the amino acid's vibrational dynamics. Evidently, large-scale conformational changes due to rotational motion often result in temporary restrictions in local vibrational motions [42]. The inverse correlation between MSD and AC at 180° depicted in Fig. 2E elucidates the interplay between conformational changes from UV-induced rotational motion and local vibrational motions in amino acids. Thus, ED spectrometry offers insights into amino acid structural characterizations without significantly altering their

inherent conformations. These results support the reliability of ED spectrometry for examining amino acid structural characteristics with minimal stability disruption.

3.2. Structural characterization of macro biomolecules: proteins

Proteins are complex macromolecules with diverse structures and functions, highly dependent on their conformation [43]. Assessing protein structural characteristics in cancer biology is critical to understanding cancer mechanisms, including progression and treatment resistance [44]. We extended the applicability of ED spectrometry in AS mode to investigate the structure change in standard reference proteins with different stereochemical characteristics, specifically BSA, avidin, chymotrypsin, and xylanase (Fig. S2). Each protein under investigation carries a distinct secondary structure contributing to its overall conformation. BSA, a major plasma protein with abundant α -helices, can undergo structural changes upon UV exposure, disrupting the hydrogen bonds that maintain the helices, potentially leading to their loss and a transition to a more unordered or random coil state [45]. Occasionally, the protein may reorganize into β -sheet structures. Avidin is a biotin binding tetrameric protein that is predominantly β -sheet rich. Exposure to UV light can lead to the breakdown of these structures, again leading to a more unordered state. Chymotrypsin, an enzyme with complex secondary and tertiary structures, may experience structural disruption and potential catalytic activity loss upon UV exposure [46]. Similarly, xylanase, an enzyme that degrades the polysaccharide xylan and comprises α -helices and β -sheets, can undergo structural transformations affecting enzyme activity due to UV exposure.

We employed ED spectrometry to measure the structural features in proteins. These proteins can exhibit conformational changes under various conditions, including UV exposure [47]. The AC at 180° measurement, as shown in Fig. 3A and S11, was used to assess these structural changes in proteins (Fig. S8). We then correlated the AC at 180° results with the Ab-AUC results from the UV spectrophotometer (Fig. 3B and S5) and the MSD calculated by molecular dynamics simulation at 10 ps as this time marks the start of molecular diffusion (Fig. 3C and S9) to determine the relationship between absorption and AC change. In proteins, the structural transformation under UV exposure becomes even more intricate due to the complex interactions between constituent amino acid chains held together by peptide bonds. A change in one part of the protein can lead to structural shifts in other regions, known as allostery [48]. The resulting alterations can profoundly impact the overall structure and function of proteins. BSA showed high AC at 180° and Ab-AUC values, effectively absorbs UV light, and exhibits minimal post-exposure structural changes. This is due to its abundant UV-absorbing aromatic amino acids like tryptophan, tyrosine, and phenylalanine. The protein's robust multi-domain structure and numerous disulfide bonds contribute to its low structural change [49]. Avidin and chymotrypsin display moderate AC at 180° and Ab-AUC values. Avidin's moderate Ab-AUC value primarily stems from several tryptophan residues, non-covalent subunit interactions, and biotin-binding activity. Chymotrypsin, with its dominant β-sheet structure undergoes fewer structural changes than avidin and xylanase [50]. Its moderate Ab-AUC is likely due to fewer aromatic residues than BSA and avidin. Xylanase, characterized by its unique triosephosphate isomerase (TIM) barrel folding and fewer UV-absorbing aromatic residues [51], exhibits the lowest Ab-AUC among the proteins studied. Despite its capacity for UV absorption, the distinctive structure and less abundant aromatic residues could result in higher absorbed energy per residue, potentially increasing the odds of structural alterations and

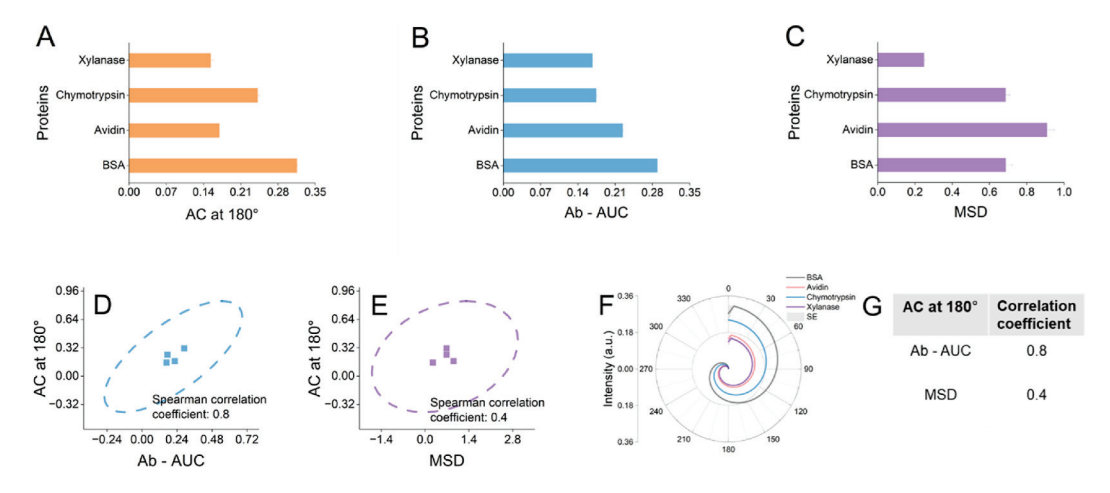


Figure 3. Structural characterization of biomacromolecules: proteins. Structural analysis of BSA, avidin, chymotrypsin, and xylanase. (A) AC at 180° , indicating structural changes in proteins due to UV elliptical polarized light absorption. (B) Experimental absorption (Ab-AUC), validating structural alterations due to absorption. (C) MSD results at 10ps, highlighting protein vibrational motion and stability dynamics. (D) Spearman correlation coefficient of 0.8 between AC at 180° and Ab-AUC, within a 95 % confidence ellipse, indicates a strong positive correlation, highlighting the interplay between structural change and absorption properties in proteins. (E) Spearman correlation coefficient of 0.4 between AC at 180° and MSD, within a 95 % confidence ellipse, suggests a moderate positive correlation, indicating that higher AC values align with increased atomic vibrational motion, influenced by protein properties like bonding patterns and folding mechanisms. (F) AC diagrams for proteins, depicting structural transformations as captured in differential AC peaks. (G) Summarizes Spearman correlation coefficients, correlating AC at 180° with both Ab-AUC and MSD. The ED spectra for AC were averaged from five repeated measurements. Error bars, mean \pm s.e.m; n=4.

making xylanase susceptible to UV-induced changes. The correlation study between the AC at 180° and Ab-AUC values revealed a Spearman correlation coefficient of 0.8, as depicted in Fig. 3D and G. This relationship suggests that proteins rich in aromatic residues such as tryptophan, tyrosine, and phenylalanine are better equipped to absorb and dissipate UV energy, protecting their structure as reflected in higher AC at 180° values. Conversely, proteins with fewer such residues have a lower UV absorption capacity leading to a greater potential for structural changes upon UV exposure due to the higher energy absorption per residue, reflecting lower AC at 180° values. Therefore, AC indirectly indicates a protein's structural resilience upon UV exposure. Furthermore, this high correlation signifies that ED spectrometry and UV spectrophotometry effectively capture similar structural changes in the proteins.

To further evaluate the relation between structural dynamics and AC, we employed the MSD method to measure molecule displacement for characterizing molecular vibrational motion [52]. The correlation study between AC at 180° and MSD values across four proteins yielded a Spearman correlation coefficient of 0.4, indicating a moderate positive correlation as shown in Fig. 3E and G. This suggests that higher AC at 180° values typically align with a moderate increase in atomic vibrational motion, as indicated by MSD values. However, vibrational motion responses depend on intrinsic protein properties like bonding patterns, folding mechanisms, and overall structure. For instance, BSA, despite higher vibrational motion, retains structural integrity, potentially due to hydrogen bond disruption in the α -helix structure. This disruption triggers a conformational change, facilitating a transition to a more stable β -sheet structure [53]. Likewise, avidin, characterized by its tetrameric structure, displays moderate structural stability alongside the highest vibrational motion. This suggests that avidin's unique inter-subunit interactions may enable it to withstand considerable molecular motion without significant structural alterations. Lastly, chymotrypsin and xylanase display less vibrational motion but undergo more structural changes, possibly due to their unique folding patterns and fewer aromatic residues. This makes them more prone to structural changes, as captured in differential AC which illustrates structural transformations as shown in Fig. 3F. For proteins, higher MSD might not necessarily indicate extensive structural change. Instead, it may reflect protein flexibility, with frequent conformational changes and folding-unfolding events inherent to their biological function.

Our study confirms the utility of ED spectrometry in revealing UV-induced protein structural characterizations. The correlation analysis offers a comprehensive understanding of protein transformations. Therefore, utilizing ED spectrometry for studying protein structural characteristics bolsters stereochemical analysis and generates insights valuable to biophysics and structural cancer biology research.

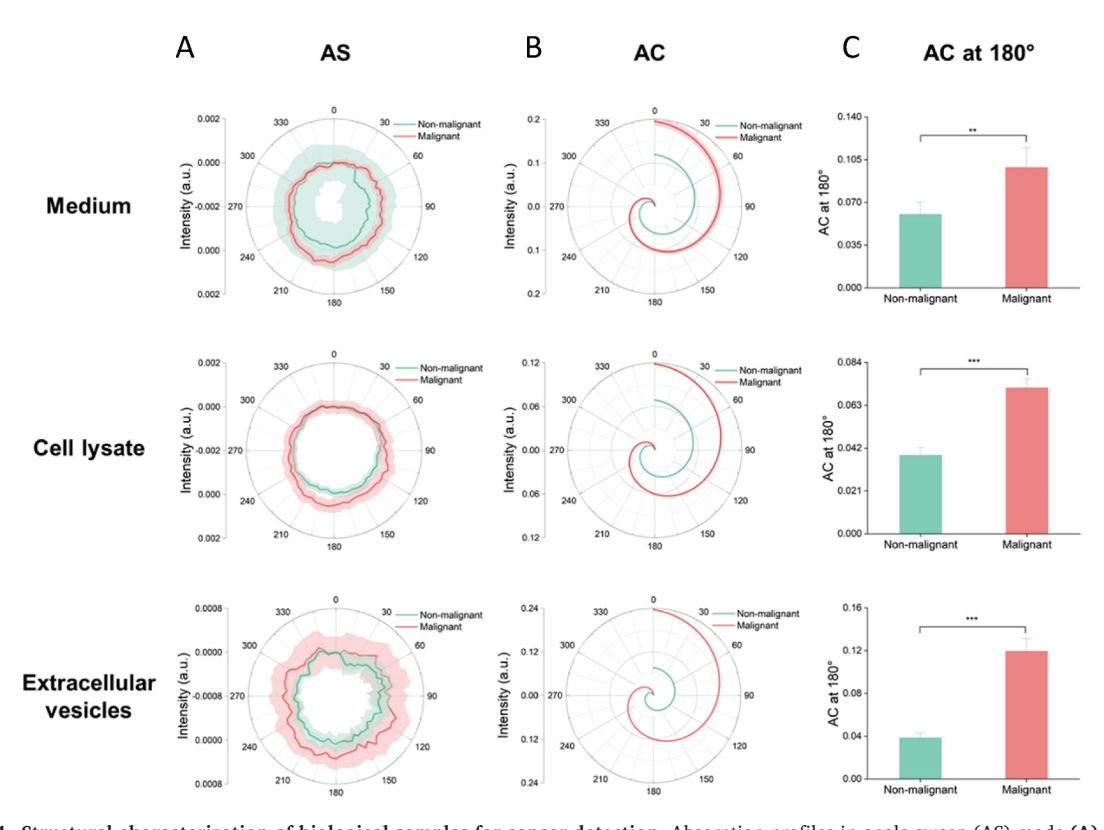


Figure 4. Structural characterization of biological samples for cancer detection. Absorption profiles in angle sweep (AS) mode (A), AC (B), and AC at 180° (C) illustrating structural changes in non-malignant and malignant samples, at medium, cell lysates, and extracellular vesicles level. The AS data highlights absorption characteristics, while AC metrics reveal structural variations, particularly due to the β-sheet richness in malignant samples. Error bars, mean \pm s.e.m; n=4. Non-malignant: HPNE, Malignant: MIA PaCa-2. p-values were determined by unpaired two-tailed t-tests from measurements collected from five biological repeats per sample, N=5. Statistical significance was denoted as follows: *p<0.05, **p<0.01, ***p<0.001, and ****p<0.0001.

3.3. Structural characterization of biological samples for cancer detection

The status of tumor differentiation is a crucial parameter in cancer biology, significantly influencing disease progression and patient prognosis [54]. The degree of differentiation often correlates with the inherent aggressive behavior of the tumor, offering potential as a unique diagnostic marker [55]. Therefore, the ability to effectively discriminate between malignant and non-malignant states using stereochemical characterization represents an imperative goal in contemporary oncology. Our previous study has revealed a significant presence of β -sheet structures in malignant cells and their EVs, potentially serving as a biomarker for cancer [13]. This study finds that β -sheet richness is a trait of cancerous cells and their EVs. To further investigate, we aimed to explore this avenue by probing the differential conformation of non-malignant (HPNE) and malignant (MIA PaCa-2) samples. We employed ED spectrometry that discerned conformational changes within biological macro- and micro-molecules. The experimental protocol involved capturing ED spectra in AS mode from biological samples, namely, the cell medium, cell lysate, and EVs illustrated in Fig. 4 and S3. These components encapsulate the collective structural attributes of the samples, offering holistic insights into conformational changes. We analyzed the spectra obtained from an AS mode using AC analysis (Figs. S2 and S12). This method allows us to examine the absorption asymmetry, indicating structural alterations in the sample.

Our results highlighted an absolute contrast between the non-malignant and malignant samples at medium, cell lysate, and EVs level. The malignant MIA PaCa-2 medium demonstrated a significant difference in AS (Fig. 4), potentially due to the secreted EVs from the malignant cell that are β -sheet rich. Distinct AS differences observed in cell lysates and EVs can discriminate the malignant samples from non-malignant ones due to their enriched β-sheet secondary structures. We subjected the samples to AC analysis, which revealed distinct AC values for malignant and non-malignant samples. The malignant samples demonstrated higher AC values. This difference likely arises from the variations in secondary structures, particularly the abundance of β-sheets, in the malignant MIA PaCa-2 samples (Fig. 4). Substantiating this finding, the AC analysis further differentiated the cell types on medium, cell lysate, and EVs level. The malignant counterparts showed a higher AC, pointing to minimal structural variation potentially due to the structure's rich in β -sheets, which contain an extensive inter-strand hydrogen bonding network that forms between the protein backbone's carbonyl oxygen atoms and the amide hydrogen atoms [56]. This hydrogen bonding network creates a rigid and planar structure less susceptible to structural changes, leading to a higher AC value in the malignant counterparts. Whereas the non-malignant samples having a lower AC indicate substantial conformational modifications. It is reasonable that these samples contain a higher proportion of α -helices, which are generally less steady than β -sheets due to fewer hydrogen bonds and more flexibility. Further, we deployed AC at 180° analysis to quantify the extent of structural transformations within the biological samples (Fig. S12). The malignant MIA PaCa-2 samples exhibited a higher AC at 180° value than the non-malignant HPNE samples at the medium, cell, and EV levels, reinforcing the low conformational change inherent to the malignant state illustrated in Fig. 4.

Our finding confirms that a comprehensive interpretation of AS, AC, and AC at 180° analyses can offer a reliable and distinctive evaluation for distinguishing between non-malignant and malignant states. This study elucidates the potential of these methodologies as potent tools for monitoring tumor differentiation. By offering a clear understanding of tumor behavior at the structural level of biomolecules, these approaches could significantly advance noninvasive cancer detection methods. The study demonstrates the efficacy of the ED method in differentiating malignant from non-malignant samples. Its compact and user-friendly design, compared to traditional CD spectrometers, suggests significant potential for clinical diagnostics. However, for clinical applications targeting tumorous EVs in the circulatory system, isolation or enrichment steps may still be required. The current ED spectrometer, particularly adept at biomolecular structure characterization, requires further refinement for effective clinical use. This research lays the groundwork for its development into a comprehensive diagnostic tool for cancer.

3.4. Is absorption coefficient polarization-dependent?

We previously developed an ED spectrometer that incorporates a waveplate and linear polarizer to generate elliptically polarized incident light, and in this study, we integrated AC as a structural characterization method. Surprisingly, our findings revealed a phenomenon that contradicts the theoretical deduction. To illustrate this contradiction, we established a mathematical model based on classical optics as follows:

Since the zero-order magnesium fluoride waveplate at 214 nm was used, a linear model was used for simulation:

$$\Phi(\lambda) = 53.5 \frac{2\pi}{\lambda}$$
;

The equation models the phase shift (Φ) introduced by waveplate. Here, 53.5 represents the constant phase shift, and $\frac{2\pi}{\lambda}$ converts wavelength to angular frequency.

To model the polarization-dependent absorbance of the sample, we describe the sample by the Mueller matrix $M_{sample} = M_{lb} M_{cb} M_{ld}$ M_{cd} , where M_{lb} , M_{cb} , M_{ld} , and M_{cd} are the Mueller matrices describing the linear birefringence (LB), circular birefringence (CB), and linear dichroism (LD) properties of the sample, respectively [57]. For simulation simplicity, we ignored the matrices except M_{cd} . The M_{cd} was defined as,

$$egin{aligned} egin{aligned} egin{aligned} M_{cd}\left(\lambda
ight) = \left(egin{array}{cccc} a(\lambda) & 0 & 0 & CD(\lambda) \ 0 & a(\lambda) & 0 & 0 \ CD(\lambda) & 0 & 0 & a(\lambda) \end{array}
ight) \end{aligned}$$

where, $CD(\lambda)$ was derived from CD measurements.

The output Stokes vector is calculated as $S_{sample} = M_{CD} \times M_{wpr} \times S_i$ where $Si(\lambda)$ was the emergent Stokes vector of the linear polarizer and is given by

$$S_{i}(\lambda) = I_{0}(\lambda) \begin{pmatrix} 1 \\ -1 \\ 0 \\ 0 \end{pmatrix}$$

Mueller matrix of the rotating waveplate was constructed as [58],

$$\begin{aligned} \mathbf{\textit{M}}_{\textit{wpr}}(\boldsymbol{\varPhi},\boldsymbol{\theta}) = \begin{pmatrix} 1 & 0 & 0 & 0 \\ 0 & \cos^2\theta + \cos\boldsymbol{\varPhi}\sin^2\theta & (1-\cos\boldsymbol{\varPhi})\sin\boldsymbol{\theta}\cos\boldsymbol{\theta} & -\sin\boldsymbol{\varPhi}\sin\boldsymbol{\theta} \\ 0 & (1-\cos\boldsymbol{\varPhi})\sin\boldsymbol{\theta}\cos\boldsymbol{\theta} & \sin^2\theta + \cos\boldsymbol{\varPhi}\cos^2\theta & \sin\boldsymbol{\varPhi}\cos\boldsymbol{\theta} \\ 0 & \sin\boldsymbol{\varPhi}\sin\boldsymbol{\theta} & -\sin\boldsymbol{\varPhi}\cos\boldsymbol{\theta} & \cos\boldsymbol{\varPhi} \end{pmatrix} \end{aligned}$$

Doing summation of output Stokes vector over the broadband wavelengths of 200–260 nm restricted by the available *CD* measurement data, the transmission intensity of the sample $I_{sample}(\theta)$ can be obtained from the first Stokes parameter of the summation,

$$\int S_{sample}(heta) d\lambda = egin{pmatrix} I_{sample}(heta) \ Q(heta) \ U(heta) \ V(heta) \end{pmatrix}$$

$$\int S_{blank}(heta) d\lambda = egin{pmatrix} I_{blank} \ Q_{blank}(heta) \ U_{blank}(heta) \ V_{blank}(heta) \end{pmatrix}$$

where $I_{blank}(\theta)$ was calculated using a similar procedure as, $S_{blank} = M_{wpr} \times S_i$ From the above equations, we can obtain $I_{sample}(\theta)$, as follows.

$$I_{\textit{sample}}(\theta) = \int I_0 \; (\lambda) \; a(\lambda) d\lambda - \sin(\theta) \int \left(\textit{CD}(\lambda) \times I_0 \; (\lambda) \times \sin(\theta) \times \sin\left(\frac{107\pi}{\lambda}\right) d\lambda \right) d\lambda$$

$$I_{blank}(\theta) = \int I_0(\lambda) \ d\lambda$$

The absorption is calculated with the formula below.

$$A(\theta) = log \left(\frac{I_{blank}(\theta)}{I_{sample}(\theta)} \right)$$

From $I_{sample}(\theta)$ and $I_{blank}(\theta)$ values, we can simplify $A(\theta)$ as,

$$I_{sample}(\theta) = I_{blank}(\theta) e^{-A(\theta)}$$

$$\int I_0 (\lambda) \ a(\lambda) d\lambda - \sin(\theta) \int CD(\lambda) I_0 (\lambda) \sin(\theta) \sin\left(\frac{107\pi}{\lambda}\right) d\lambda = e^{-A(\theta)} \int I_0(\lambda) \ d\lambda$$

Since $\int I_0(\lambda) \, a(\lambda) d\lambda$, $\int CD(\lambda) I_0(\lambda) sin(\theta) \, sin\left(\frac{107\pi}{\lambda}\right) d\lambda$, and $\int I_0(\lambda) \, d\lambda$ are independent of θ , we can write the above equation as

$$k_1 - k_2 \sin \theta = k_3 e^{-A(\theta)}$$

$$k_1 = k_2 \sin(\theta) + k_3 e^{-A(\theta)}$$

where,

$$k_1 = \int I_0 (\lambda) a(\lambda) d\lambda$$

$$k_2 = \int CD(\lambda) \ I_0 \ (\lambda) \ sin(\theta) \ sin\left(\frac{107\pi}{\lambda}\right) d\lambda$$

And
$$k_3 = \int I_0(\lambda) d\lambda$$

From the above equation, we can see that a (λ) is independent of θ .

Our study examined the absorption characteristics of biological samples, revealing a discrepancy between empirical findings and theoretical math deduction. Contrary to our findings from math deduction above, it was found experimentally that the data suggests absorbance varies with structural attributes and incident angle. The dependency was noted across amino acids, proteins, and malignant samples. The above theoretical deduction, based on a Mueller matrix-based model, assumed that the absorption coefficient a (λ) is independent of the incident angle θ . In contrast, our experimental data demonstrated that absorbance varies with structural attributes and incident polarization. This divergence underscores the limitations of the existing theoretical model and emphasizes the need for a more refined simulation approach that accurately represents the complex absorption behavior of structurally diverse biological samples. Future work should focus on the impact of molecular structure and orientation on absorption, to bridge the gap between theoretical results and experimental findings.

4. Discussion

Previously, we have developed and tested our novel ED spectrometer and justified its use for stereochemical analysis. Comparing it to CD spectrometer which it is most closely related to, the ED spectrometer measures difference in absorption between left and right elliptically polarized light. The defined ED value helps to reduce individual measurement bias from the instrument, however, due to mechanical moving components within our ED spectrometer, noise in measurements is inevitable. Integration of Autocorrelation which is a statistical method to reduce noise was therefore used. With this reduction in noise due to addition of statistical analysis method, AC at 180 can be derived as an indicator for molecule symmetry in response to left and right elliptically polarized light, aligning this value more closely to the true structure of the molecule. Furthermore, our study explored the complexity of the structural characteristics of biological molecules under UV light exposure. The research posed two fundamental questions. First, whether the structural changes in biological molecules can be detected and quantified accurately utilizing our ED spectrometer integrated with AC analysis. Second, if these changes can offer an observable characteristic between non-malignant and malignant samples, aiding in noninvasive cancer diagnosis. Addressing the first question, we devised a robust methodology to detect and quantify structural changes in biological molecules, employing the AC function on ED spectra in conjunction with a correlation study involving Ab-AUC, Ab sim-AUC, and MSD. The strategy used a correlation of AC at 180°, indicating structural changes upon UV light exposure. Compared to CD spectrometry, which outputs one value readout, this value offers further insight into structural changes of a molecule within sample. Investigating amino acids offered our findings that confirmed a detectable change in the structural behavior of aromatic and nonaromatic amino acids upon UV exposure, providing an initial validation of the ED spectrometry without significantly disrupting the stability of amino acids as detected by MSD. In proteins, given their structural complexity and relevance in disease progression. The proteins tested exhibited differential structural characteristics, reflecting the extent of conformational change related to their secondary structure constituents, further validating our methodology. Our focus then shifted to exploring the structural characteristics of biological samples to contribute to the evolving landscape of tumor differentiation and cancer diagnosis. The study discerned contrasting conformational behaviors between non-malignant and malignant cells. The malignant samples exhibited a low conformational change, as evidenced by a higher AC value, reinforcing the positive correlation between β -sheet rich secondary structure and malignancy status. This insight has substantial implications for oncology, offering a reliable and distinctive tool for discriminating malignant from non-malignant states and monitoring tumor differentiation. Nevertheless, our study also revealed a discrepancy between theoretical and experimental findings in absorption properties. Contrary to the simplifying assumption in the classical theoretical model that absorption a (λ) is independent of the angle of incidence θ , the absorption behavior observed in our study is dependent to the polarization variation and the structures of the samples. Future work should explore the reasons behind these structural transformations in malignant clinical samples and delineate the proteins responsible for tumor initiation and progression in the patient cohorts. This study establishes a foundational framework for utilizing the ED method in cancer diagnostics, acknowledging the need for further refinement to enhance its sensitivity, specificity, and diagnostic accuracy. Recognizing the ED method's potential, we are focused on developing it as a competitive tool for cancer detection and for its use as an alternative to the CD spectrometer in clinical settings for specific structural analyses. It currently demonstrates promise in biomolecular characterization, particularly in distinguishing malignant cells and their exosomal structures from non-malignant counterparts, suggesting significant implications for its application in clinical diagnostics. Limitations of the ED spectrometer in its current version have addressed sources of error due to noise by integrating Autocorrelation data analysis method which results in more reproducible measurements while also offering quick and easy data analysis by use of data analysis software's such as MATLAB and OriginPro. Furthermore, asymmetries and discrepancies in mechanical component parts such as quarter waveplate and motorized rotator are accounted for during measurements and data analysis by use of blank and sample repeat measurements. With use of precise rotator and mounting onto an aluminum breadboard, discrepancies are kept consistent throughout all measurements allowing for absorbance values of sample to be normalized to blank measurements. Future trends involve further sample testing from various sources such as saliva, serum, or plasma, as well as testing further clinical utility by samples of malignant biomarkers in a non-malignant background. Trends also include testing ED spectrometer's ability to differentiate DNA from malignant and non-malignant sources, as well as testing samples with known structural alterations such as systemic amyloidosis, which will provide a wider application for this technology.

Our research deepens the understanding of the structural characteristics of biological molecules and their role as potential biomarkers for cancer. By concentrating on collective attributes, such as the increased presence of β -sheets in cancerous cells and EVs, we suggest a refined diagnostic approach [13–15]. Our AC method, combined with the ED spectrometer, broadens the scope of stereochemical analyses, creating a multifaceted tool for structural characterization. This approach can detect structural changes in biomolecules associated with disease, potentially offering a reliable, noninvasive technique for cancer detection, thereby enhancing

patient prognosis.

Data and materials availability

All data are available in the main text or supplementary materials.

CRediT authorship contribution statement

Yusuf Asad: Writing – review & editing, Writing – original draft, Investigation. Keerthi Priya Jangili: Writing – review & editing, Investigation. Amara Arshad: Writing – review & editing, Formal analysis. Maliha Elma: Investigation. Komila Rasuleva: Investigation. Alfred Akinlalu: Writing – review & editing. Tommy Gao: Writing – review & editing. Umamaheswara Rao Tida: Writing – review & editing. Wenjie Xia: Writing – review & editing, Formal analysis. Dali Sun: Writing – review & editing, Supervision, Software, Project administration, Methodology, Funding acquisition, Conceptualization.

Declaration of competing interest

The authors declare no conflict of interest.

Acknowledgments

The authors acknowledge North Dakota State University Center for Computationally Assisted Science and Technology for computing resources. This work was financially supported by grants from the National Cancer Institute (R03CA252783, R21CA270748) and the National Institute of General Medical Sciences (U54GM128729) of National Institutes of Health to DS, National Science Foundation CAREER Award (2236885) to DS, NDSU EPSCOR STEM Research and Education fund (FAR0032086) to DS, ND EPSCOR: Advancing Science Excellence in ND (FAR0030554) to DS, National Science Foundation (NSF) under NSF EPSCOR Track-1 Cooperative Agreement (OIA #1355466) to DS. National Science Foundation (NSF) under NSF CAREER Award (No. 2237063) to WX, NDSU Foundation and Alumni Association to DS, Colorado Office of Economic Development and International Trade Advance Industries Proof of Concept award to DS.

Appendix A. Supplementary data

Supplementary data to this article can be found online at https://doi.org/10.1016/j.heliyon.2024.e38399.

References

- [1] M. Colombo, G. Raposo, C. Théry, Biogenesis, Secretion, and Intercellular Interactions of Exosomes and Other Extracellular Vesicles 30 (2014) 255–289, https://doi.org/10.1146/ANNUREV-CELLBIO-101512-122326.
- [2] L. Konermann, S. Vahidi, M.A. Sowole, Mass spectrometry methods for studying structure and dynamics of biological macromolecules, Anal. Chem. 86 (2014) 213–232, https://doi.org/10.1021/AC4039306/ASSET/IMAGES/LARGE/AC-2013-039306_0011. JPEG.
- [3] S. Suresh, Biomechanics and biophysics of cancer cells, Acta Biomater. 3 (2007) 413, https://doi.org/10.1016/J.ACTBIO.2007.04.002.
- [4] R. Chaudhuri, Y. Cheng, C.R. Middaugh, D.B. Volkin, High-throughput biophysical analysis of protein therapeutics to examine interrelationships between aggregate formation and conformational stability, AAPS J. 16 (2014) 48–64, https://doi.org/10.1208/S12248-013-9539-6/FIGURES/9.
- [5] R.J.D. Miller, Femtosecond crystallography with ultrabright electrons and x-rays: capturing chemistry in action, Science 343 (2014) 1108–1116, https://doi. org/10.1126/SCIENCE.1248488/ASSET/67E3F73D-A436-4203-AF45-42E4D2BD353F/ASSETS/GRAPHIC/343_1108_F5.JPEG, 1979.
- [6] A.K. Mittermaier, L.E. Kay, Observing biological dynamics at atomic resolution using NMR, Trends Biochem. Sci. 34 (2009) 601–611, https://doi.org/10.1016/ J.TIBS.2009.07.004.
- [7] K.M. Yip, N. Fischer, E. Paknia, A. Chari, H. Stark, Atomic-resolution protein structure determination by cryo-EM, Nature 587 (7832 587) (2020) 157–161, https://doi.org/10.1038/s41586-020-2833-4, 2020.
- [8] O. Ozohanics, A. Ambrus, Hydrogen-deuterium exchange mass spectrometry: a novel structural biology approach to structure, dynamics and interactions of proteins and their complexes. Life 10 (2020) 286. https://doi.org/10.3390/LIFE10110286, 286 10 (2020).
- [9] G. Zandomeneghi, M.R.H. Krebs, M.G. McCammon, M. Fändrich, FTIR reveals structural differences between native β-sheet proteins and amyloid fibrils, Protein Sci. 13 (2004) 3314. https://doi.org/10.1110/PS.041024904.
- [10] S. Doose, H. Neuweiler, M. Sauer, Fluorescence quenching by photoinduced electron transfer: a reporter for conformational dynamics of macromolecules, ChemPhysChem 10 (2009) 1389–1398, https://doi.org/10.1002/CPHC.200900238.
- [11] S. Kelly, N. Price, The use of circular dichroism in the investigation of protein structure and function, Curr. Protein Pept. Sci. 1 (2000) 349–384, https://doi.org/10.2174/1389203003381315.
- [12] A. Bauer, S. Elamurugan, S.T. Selim, Fatima, E. Nega, I.T. Lima, W. Xia, D. Sun, A portable elliptical dichroism spectrometer targeting secondary structural features of tumorous protein for pancreatic cancer detection, Biosens. Bioelectron. 222 (2023) 114934, https://doi.org/10.1016/J.BIOS.2022.114934.
- [13] K. Rasuleva, S. Elamurugan, A. Bauer, M. Khan, Q. Wen, Z. Li, P. Steen, A. Guo, W. Xia, S. Mathew, R. Jansen, D. Sun, β-Sheet richness of the circulating tumor-derived extracellular vesicles for noninvasive pancreatic cancer screening, ACS Sens. 6 (2021) 4489–4498, https://doi.org/10.1021/ACSSENSORS.1C02022/ASSET/IMAGES/LARGE/SE1C02022 0004, JPEG.
- [14] K. Rasuleva, K.P. Jangili, A. Akinlalu, A. Guo, P. Borowicz, C. Li, D. Sun, EvIPqPCR, target circulating tumorous extracellular vesicles for detection of pancreatic cancer, Anal. Chem. 95 (2023) 10353–10361, https://doi.org/10.1021/ACS.ANALCHEM.3C01218/ASSET/IMAGES/LARGE/AC3C01218_0004.JPEG.
- [15] D. Sun, Z. Zhao, S. Spiegel, Y. Liu, J. Fan, P. Amrollahi, J. Hu, C.J. Lyon, M. Wan, T.Y. Hu, Dye-free spectrophotometric measurement of nucleic acid-to-protein ratio for cell-selective extracellular vesicle discrimination, Biosens. Bioelectron. 179 (2021) 113058, https://doi.org/10.1016/J.BIOS.2021.113058.

[16] J. VandeVondele, P. Tröster, P. Tavan, G. Mathias, Vibrational spectra of phosphate ions in aqueous solution probed by first-principles molecular dynamics, J. Phys. Chem. 116 (10) (2012) 2466–2474.

- [17] R. Sivaraj, P.K. Rahman, P. Rajiv, H.A. Salam, R. Venckatesh, Biogenic copper oxide nanoparticles synthesis using Tabernaemontana divaricate leaf extract and its antibacterial activity against urinary tract pathogen, Spectrochim. Acta Mol. Biomol. Spectrosc. 133 (2014) 178–181.
- [18] K. Guo, N. Ji, F. Han, Q. Yang, N. Wang, C. Miao, Biomass-based ionic liquids efficiently catalyzed the cycloaddition reaction of epoxides with CO 2 by hydrogen-bonding and the anion cooperative effect. RSC Sustainability 2 (4) (2024) 1074–1080.
- [19] Y. Ding, X.C. Li, D. Ferreira, Theoretical calculation of electronic circular dichroism of the rotationally restricted 3,8"-biflavonoid morelloflavone, J. Org. Chem. 72 (2007) 9010–9017, https://doi.org/10.1021/J0071134Z/SUPPL_FILE/J0071134Z-FILE003.PDF.
- [20] P.J. Stephens, N. Harada, ECD cotton effect approximated by the Gaussian curve and other methods, Chirality 22 (2010) 229–233, https://doi.org/10.1002/ CHIR.20733.
- [21] J. Huang, S. Rauscher, G. Nawrocki, T. Ran, M. Feig, B.L. De Groot, H. Grubmüller, A.D. MacKerell, CHARMM36m: an improved force field for folded and intrinsically disordered proteins, Nat. Methods 14 (2017) 71, https://doi.org/10.1038/NMETH.4067.
- [22] M.B. Kubitzki, B.L. De Groot, Molecular dynamics simulations using temperature-enhanced essential dynamics replica exchange, Biophys. J. 92 (2007) 4262–4270, https://doi.org/10.1529/BIOPHYSJ.106.103101.
- [23] A. Akinlalu, Z. Flaten, K. Rasuleva, M.S. Mia, A. Bauer, S. Elamurugan, D. Sun, Integrated proteomic profiling identifies amino acids selectively cytotoxic to pancreatic cancer cells, Innovation 5 (3) (2024), https://doi.org/10.1016/j.xinn.2024.100626.
- [24] A. Berthod, Chiral recognition mechanisms, Anal. Chem. 78 (2006) 2093–2099, https://doi.org/10.1021/AC0693823/ASSET/AC0693823.FP.PNG_V03.
- [25] H.F. Ji, A general method to predict optical rotations of chiral molecules from their structures, RSC Adv. 13 (2023) 4775–4780, https://doi.org/10.1039/ D2RA08290J.
- [26] N.J. Anthis, G.M. Clore, Sequence-specific determination of protein and peptide concentrations by absorbance at 205 nm, Protein Sci. 22 (2013) 851, https://doi.org/10.1002/PRO.2253.
- [27] S. Prasad, I. Mandal, S. Singh, A. Paul, B. Mandal, R. Venkatramani, R. Swaminathan, Near UV-Visible electronic absorption originating from charged amino acids in a monomeric protein, Chem. Sci. 8 (2017) 5416–5433, https://doi.org/10.1039/C7SC00880E.
- [28] Q. Song, Z. Cheng, M. Kariuki, S.C.L. Hall, S.K. Hill, J.Y. Rho, S. Perrier, Molecular self-assembly and supramolecular chemistry of cyclic peptides, Chem Rev 121 (2021) 13936–13995, https://doi.org/10.1021/ACS.CHEMREV.0C01291/ASSET/IMAGES/MEDIUM/CR0C01291 0043.GIF.
- [29] P.R. Callis, T. Liu, Quantitative prediction of fluorescence quantum yields for tryptophan in proteins, J. Phys. Chem. B 108 (2004) 4248–4259, https://doi.org/10.1021/JP0310551/ASSET/IMAGES/MEDIUM/JP0310551E00008.GIF.
- [30] M. Brandl, M.S. Weiss, A. Jabs, J. Sühnel, R. Hilgenfeld, C-h···π-interactions in proteins, J. Mol. Biol. 307 (2001) 357–377, https://doi.org/10.1006/ JMBI 2000 4473
- [31] G.G. Hammes, S.J. Benkovic, S. Hammes-Schiffer, Flexibility, diversity, and cooperativity: pillars of enzyme catalysis, Biochemistry 50 (2011) 10422–10430, https://doi.org/10.1021/BI201486F/ASSET/IMAGES/LARGE/BI-2011-01486F_0005. JPEG.
- [32] G.H. Beaven, E.R. Holiday, Ultraviolet absorption spectra of proteins and amino acids, Adv. Protein Chem. 7 (1952) 319–386, https://doi.org/10.1016/S0065-3233(08)60022-4.
- [33] C. Bissantz, B. Kuhn, M. Stahl, A medicinal chemist's guide to molecular interactions, J. Med. Chem. 53 (2010) 5061–5084, https://doi.org/10.1021/ JM100112J/SUPPL FILE/JM100112J SI 001.PDF.
- [34] T. Mori, Y. Inoue, S. Grimme, Time dependent density functional theory calculations for electronic circular dichroism spectra and optical rotations of conformationally flexible chiral donor-acceptor dyad, J. Org. Chem. 71 (2006) 9797–9806, https://doi.org/10.1021/J00618551.
- [35] L. Li, I. Vorobyov, T.W. Allen, The different interactions of lysine and arginine side chains with lipid membranes, J. Phys. Chem. B 117 (2013) 11906, https://doi.org/10.1021/JP405418Y.
- [36] J.C. Aledo, Methionine in proteins: the Cinderella of the proteinogenic amino acids, Protein Sci. 28 (2019) 1785, https://doi.org/10.1002/PRO.3698.
- [37] K.M. Makwana, R. Mahalakshmi, Implications of aromatic-aromatic interactions: from protein structures to peptide models, Protein Sci. 24 (2015) 1920, https://doi.org/10.1002/PRO.2814.
- [38] G. Schiró, C. Caronna, F. Natali, A. Cupane, Direct evidence of the amino acid side chain and backbone contributions to protein anharmonicity, J. Am. Chem. Soc. 132 (2010) 1371–1376, https://doi.org/10.1021/JA908611P/ASSET/IMAGES/LARGE/JA-2009-08611P_0004.JPEG.
- [39] T.X. Xiang, B.D. Anderson, Liposomal drug transport: a molecular perspective from molecular dynamics simulations in lipid bilayers, Adv. Drug Deliv. Rev. 58 (2006) 1357–1378, https://doi.org/10.1016/J.ADDR.2006.09.002.
- [40] M. Miller, The importance of being flexible: the case of basic region leucine zipper transcriptional regulators, Curr. Protein Pept. Sci. 10 (2009) 244, https://doi.org/10.2174/138920309788452164.
- [41] M. Moosavi, N. Banazadeh, M. Torkzadeh, Structure and dynamics in amino acid choline-based ionic liquids: a combined QTAIM, NCI, DFT, and molecular dynamics study, J. Phys. Chem. B 123 (2019) 4070–4084, https://doi.org/10.1021/ACS.JPCB.9B01799/ASSET/IMAGES/MEDIUM/JP-2019-01799T_M014. GIF.
- [42] B.K. Ho, D.A. Agard, Probing the flexibility of large conformational changes in protein structures through local perturbations, PLoS Comput. Biol. 5 (2009) e1000343, https://doi.org/10.1371/JOURNAL.PCBI.1000343.
- [43] A. Karshikoff, L. Nilsson, R. Ladenstein, Rigidity versus flexibility: the dilemma of understanding protein thermal stability, FEBS J. 282 (2015) 3899–3917, https://doi.org/10.1111/FEBS.13343.
- [44] E. Sahai, I. Astsaturov, E. Cukierman, D.G. DeNardo, M. Egeblad, R.M. Evans, D. Fearon, F.R. Greten, S.R. Hingorani, T. Hunter, R.O. Hynes, R.K. Jain, T. Janowitz, C. Jorgensen, A.C. Kimmelman, M.G. Kolonin, R.G. Maki, R.S. Powers, E. Puré, D.C. Ramirez, R. Scherz-Shouval, M.H. Sherman, S. Stewart, T. D. Tlsty, D.A. Tuveson, F.M. Watt, V. Weaver, A.T. Weeraratna, Z. Werb, A framework for advancing our understanding of cancer-associated fibroblasts, Nat. Rev. Cancer 20 (2020) 174–186, https://doi.org/10.1038/s41568-019-0238-1, 3 20 (2020).
- [45] O.S. Rabotyagova, P. Cebe, D.L. Kaplan, Collagen structural hierarchy and susceptibility to degradation by ultraviolet radiation, Mater. Sci. Eng. C 28 (2008) 1420–1429, https://doi.org/10.1016/J.MSEC.2008.03.012.
- [46] A. Kumar, P. Venkatesu, Overview of the stability of α-chymotrypsin in different solvent media, Chem Rev 112 (2012) 4283–4307, https://doi.org/10.1021/CR2003773/ASSET/IMAGES/MEDIUM/CR-2011-003773 0020.GIF.
- [47] R.W. Woody, [4] Circular dichroism, Methods Enzymol. 246 (1995) 34–71, https://doi.org/10.1016/0076-6879(95)46006-3.
- [48] N.M. Goodey, S.J. Benkovic, Allosteric regulation and catalysis emerge via a common route, Nat. Chem. Biol. 4 (8 4) (2008) 474–482, https://doi.org/10.1038/nchembio.98, 2008.
- [49] V.M. Balcão, M.M.D.C. Vila, Structural and functional stabilization of protein entities: state-of-the-art, Adv. Drug Deliv. Rev. 93 (2015) 25–41, https://doi.org/10.1016/J.ADDR.2014.10.005.
- [50] K. Numata, P. Cebe, D.L. Kaplan, Mechanism of enzymatic degradation of beta-sheet crystals, Biomaterials 31 (2010) 2926–2933, https://doi.org/10.1016/J. BIOMATERIALS.2009.12.026.
- [51] A. Schmidt, A. Schlacher, W. Steiner, H. Schwab, C. Kratky, Structure of the xylanase from Penicillium simplicissimum, Protein Sci. 7 (1998) 2081–2088, https://doi.org/10.1002/PRO.5560071004
- [52] Z. Yi, Y. Miao, J. Baudry, N. Jain, J.C. Smith, Derivation of mean-square displacements for protein dynamics from elastic incoherent neutron scattering, J. Phys. Chem. B 116 (2012) 5028–5036, https://doi.org/10.1021/JP2102868/ASSET/IMAGES/LARGE/JP-2011-102868_0003. JPEG.
- [53] Y.S. Wei, S.Y. Lin, S.L. Wang, M.J. Li, W.T. Cheng, Fourier transform IR attenuated total reflectance spectroscopy studies of cysteine-induced changes in secondary conformations of bovine serum albumin after UV-B irradiation, Biopolymers 72 (2003) 345–351, https://doi.org/10.1002/BIP.10436.
- [54] R. Baghban, L. Roshangar, R. Jahanban-Esfahlan, K. Seidi, A. Ebrahimi-Kalan, M. Jaymand, S. Kolahian, T. Javaheri, P. Zare, Tumor microenvironment complexity and therapeutic implications at a glance, Cell Commun. Signal. 18 (2020) 1–19, https://doi.org/10.1186/S12964-020-0530-4, 1 18 (2020).

[55] A. Jögi, M. Vaapil, M. Johansson, S. Påhlman, Cancer cell differentiation heterogeneity and aggressive behavior in solid tumors, Ups. J. Med. Sci. 117 (2012) 217, https://doi.org/10.3109/03009734.2012.659294.
 [56] J.S. Nowick, Exploring β-sheet structure and interactions with chemical model systems, Acc. Chem. Res. 41 (2008) 1319–1330, https://doi.org/10.1021/AR800064F/ASSET/IMAGES/MEDIUM/AR-2008-00064F_0007. GIF.
 [57] T.-T.-H. Pham, Y.-L. Lo, Extraction of effective parameters of turbid media utilizing the Mueller matrix approach: study of glucose sensing. https://doi.org/10.1117/J. JPD-137-0.007709. 2013

- $1117/1. JBO.17. 9.097002,\ 2012.$
- [58] Polarized Light Dennis H, Goldstein Google Books. https://books.google.com/books? hl=en&r=&id=cAlEDwAAQBAJ&oi=fnd&pg=PT18&ots=f0pJc8cOph&sig=0WWPozpA7Zgv9zHpG1WU9fbzZkY#v=onepage&q&f=false. (Accessed 18 June 2023).